

# FABRY-PEROT IMAGING SPECTROSCOPY OF INTERACTING AND MERGING GALAXIES: NGC 3690 AND NGC 6240

JACQUELINE FISCHER

Center for Advanced Space Sensing, Naval Research Laboratory, Code 4033.4F, Washington, DC 20375-5000

HOWARD A. SMITH

Laboratory for Astrophysics, National Air and Space Museum, Smithsonian Institution, Washington, DC 20560

WILLIAM GLACCUM

Applied Research Corporation, 8201 Corporate Dr., Landover, MD 20785

**ABSTRACT** We present  $2\ \mu\text{m}$  spectroscopic images in the  $\text{H}_2\ v=1-0\ S(1)$  line, the  $\text{Br}\ \gamma$  recombination line of atomic hydrogen, and the neighboring continuum of the central regions of the galaxies NGC 3690/IC 694 and NGC 6240. Based on the morphology of these images we assess the contributions of star formation, colliding disks, and nuclear activity to the line emission.

## THE INSTRUMENT, OBSERVATIONS, AND DATA ANALYSIS

Motivated by the requirements of extragalactic imaging spectroscopy (i.e., the need for tunability to accommodate different redshifts) we have assembled an IR Fabry-Perot imaging spectrometer. We use a warm, servo-controlled Fabry-Perot etalon built by Queensgate Instruments, Ltd. in the uncollimated telescope beam directly in front of the window of the KPNO Infrared Imager (IRIM). The Fabry-Perot etalon plates are coated for the entire K-band window. Since the etalon is capacitively servoed, we provide thermostatically controlled temperature stability and purge the etalon cavity with dry nitrogen. IRIM was equipped with cold, flat-topped, order sorting filters covering the range between  $2.11 - 2.28\ \mu\text{m}$ . The FWHP Fabry-Perot bandpass was  $760\ \text{km s}^{-1}$  and was stable to  $\pm 60\ \text{km s}^{-1}$ . IRIM contains a  $62 \times 58$  InSb DRO detector array. The images were obtained on the 2.1-meter telescope with  $0.78''/\text{pixel}$ , but typical seeing was  $1.5-2.0''$ . The images were shifted by fractions of a pixel to match peak or total fluxes. Spectral calibration was done using three lines of Krypton emitted from a pen-ray lamp.

For each galaxy and spectral line, images were obtained at five spectral positions as the Fabry-Perot etalon was step-scanned through the line. These images and identical scans of calibrators were flat-fielded. The  $S(1)$  line images were flux calibrated using the integrated calibration star signals. The Brackett  $\gamma$  line images in NGC 3690 were scaled using a model atmosphere and filter correction and flux calibrated based on their continuum scan signals. Within

rectangular aperture regions at the peaks of the galactic nuclei, best fits for the intrinsic line profile were generated by varying the central velocity and width of a Gaussian profile. The line fluxes and estimated calibration errors in these selected apertures, are given in table 1. The fluxes are consistent, in general, with large beam measurements in the literature. The model fit for the S(1) line in NGC 6240 is shown in figure 1. For NGC 6240, two sets of data were obtained on two different nights. The set with the better focus quality is presented here. However we note that the line width and flux derived for the second set were higher. We have not yet resolved this discrepancy. In the three compact components of NGC 3690, A, B, and C, the lines were all unresolved except for the S(1) line in C, which appears marginally resolved. Because of our low spectral resolution, the central image contains most of the line flux. The line flux images were generated by subtracting the line peak image from the average of the two continuum images. The line flux contours are based on the assumption that the width of the line emission throughout the image is equal to the model fit. The continuum image was corrected for small contamination by the line emission, by subtracting the percentage of line emission derived from the model fit. The line and continuum images are shown in figures 2 (NGC 3690) and 3 (NGC 6240).

TABLE 1 Spatially Integrated S(1), Br  $\gamma$ , and Continuum Fluxes

Galaxy	Integrated Image Area	S(1) Line Flux <sup>1</sup> ( $10^{-21}$ W cm $^{-2}$ )	Br $\gamma$ Line Flux <sup>1</sup> ( $10^{-21}$ W cm $^{-2}$ )	Continuum (mJy)
NGC 3690A	5.5"x5.5"	6.8 $\pm$ 0.7	4.1 $\pm$ 0.4	21 $\pm$ 2
B	5.5"x7.0"	5.9 $\pm$ 0.6	3.2 $\pm$ 0.4	39 $\pm$ 4
C	4.7"x4.7"	2.0 $\pm$ 0.5	4.1 $\pm$ 0.4	10 $\pm$ 1
NGC 6240	7.8"x7.8"	19 $\pm$ 2 <sup>2</sup>		47 $\pm$ 5

<sup>1</sup>For NGC 3690, the fluxes in the apertures were generated by subtracting comparable size apertures on either side of the nuclei, to minimize the effect of imperfect flat-fielding.

<sup>2</sup>See text.

## DISCUSSION

In the NGC 3690 galaxy system, the line and continuum spectral images are similar: the strongest intensity comes from the three compact components. Most of the line and continuum flux detected in large aperture measurements is extended and doesn't show structure in our images. Relative to the total flux, the infrared line and continuum fluxes of the individual components are similar to those seen in the 10  $\mu$ m and radio continua. The fact that these other probes have been found to be surprisingly consistent with starburst models (Gehrz, Sramek, and Weedman 1983) suggests that the H<sub>2</sub> line emission is emitted from individual star forming regions and supernova remnants, and not from colliding

Fig. 1. The S(1) line profile in the central  $7.8'' \times 7.8''$  in NGC 6240. The integrated intensity and statistical errors are plotted at the five spectral positions observed. The solid line is the instrumental profile as measured on a lamp line. The dashed line is the best fit to the data, derived by convolving a  $450 \text{ km s}^{-1}$  Gaussian profile with the Fabry-Perot theoretical profile (see text).

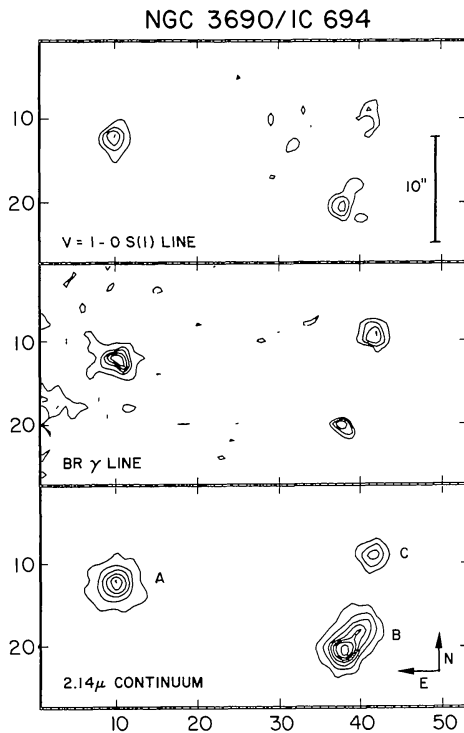
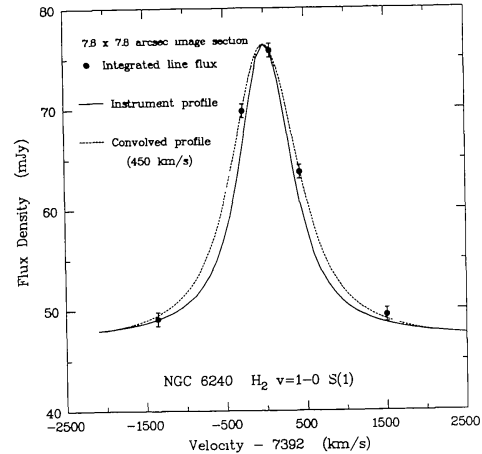


Fig. 2. S(1) line, Br  $\gamma$  line, and narrowband continuum images in NGC 3690. The contour intervals are  $1.1 \times 10^{-4}$  and  $0.55 \times 10^{-4} \text{ ergs s}^{-1} \text{ cm}^{-2} \text{ ster}^{-1}$  and  $2.2 \times 10^7 \text{ Jy ster}^{-1}$  respectively. The lowest contours are 3, 2, and 5 times the rms noise respectively.

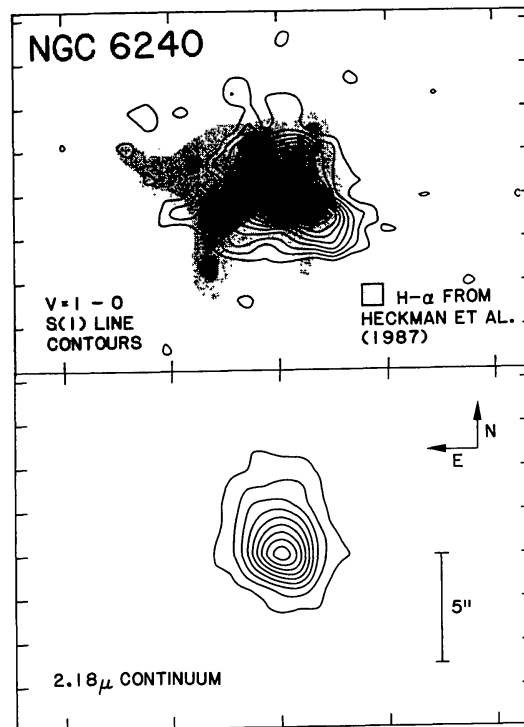


Fig. 3. S(1) line and continuum images in NGC 6240. The S(1) line image is superposed on an  $\text{H}\alpha + [\text{NII}]$  line image obtained by Heckman *et al.* (1987). The images were aligned by matching positions of the R-band and our continuum peaks. The contour interval for the line image is  $3.2 \times 10^{-5} \text{ ergs s}^{-1} \text{ cm}^{-2} \text{ ster}^{-1}$  ( $1 \sigma$ ), with the first contour equal to twice the interval. The continuum intervals are  $3.2 \times 10^6 \text{ Jy ster}^{-1}$  ( $5 \sigma$ ).

disks or active nuclei, in this interacting system. In a starburst scenario, the resemblance between the line and continuum images can be explained by the fact that the supergiant population dominates the  $2\ \mu\text{m}$  flux. The variations in the relative strengths of the various diagnostics in the different components could then be explained by differences in starburst age and IMF, as discussed in detail by Nakagawa *et al.* (1989). Additionally, our observed narrow Brackett  $\gamma$  line widths do not indicate the presence of embedded active galactic nuclei.

In contrast, the morphology of the S(1) line emission in NGC 6240 is substantially different from the  $2\ \mu\text{m}$  continuum. The continuum appears to be associated with the nuclei. The southwestern nucleus is much stronger in K-band flux than the nucleus  $1.8''$  to the northeast (see also Thronson *et al.* 1990). In figure 3 our S(1) line image is shown superposed on an image of the  $\text{H}\alpha + [\text{NII}]$  emission obtained by Heckman *et al.* (1987). Despite the differences in sensitivity and spatial resolution, the two line images both have extensions southeast, southwest and north of the southern nucleus (seen also by Herbst *et al.* 1990, in their S(1) line image). Fosbury and Wall (1979) suggest that the optical spectrum of this region is due to shocks resulting from the galaxy collision. Because of the resemblance between the S(1) and  $\text{H}\alpha + [\text{NII}]$  images and the lack of resemblance between our  $2\ \mu\text{m}$  continuum and line images, we favor such an interpretation or one in which the line emission is produced indirectly by the starburst. Heckman *et al.* argue that the  $\text{H}\alpha + [\text{NII}]$  structure may be due to the interaction between a large-scale supernovae wind and infalling molecular clouds. Draine and Woods (1990) argue that x-ray excitation from supernovae, not shocks, are responsible for the  $\text{H}_2$  emission. If this is the case, the structure seen in the S(1) line and  $\text{H}\alpha + [\text{NII}]$  line maps indicates that some of these x-rays have escaped the nuclear regions of the galaxy perpendicular to the remnant galactic disk.

## ACKNOWLEDGEMENTS

We are indebted to Ronald Probst, Richard Joyce, and the KPNO imager team for their dedicated help in using IRIM. We thank Mark Whitis, who wrote the software and built the temperature controller for the Fabry-Perot spectrometer, and came observing with us. We thank Tim Heckman and collaborators for providing a digital version of their  $\text{H}\alpha + [\text{NII}]$  image. This work was funded by the Office of Naval Research and SDIO (J.F. and W.G.) and NASA Grant NAGW-1711 (H.A.S.).

## REFERENCES

- Draine, B. T. and Woods, D. T. 1990, preprint.  
 Fosbury, R. A., E. and Wall, J. V. 1979, *M.N.R.A.S.*, **189**, 79.  
 Gehrz, R. D., Sramek, R. A., and Weedman, D. W. 1983, *A. J.*, **267**, 551.  
 Heckman, T. M., Armus, L., and Miley, G. K. 1987, *A. J.*, **92**, 276.  
 Herbst, T. M., Graham, J. R., Beckwith, S., Tsutsui, K., Soifer, B. T., and Matthews, K. 1990, preprint.  
 Nakagawa, T., Nagata, T., Geballe, T. R., Okuda, H., Shibai, H., and Matsuhara, H. 1989, *Ap. J.*, **340**, 729.  
 Thronson, H., Majewsky, S., Descartes, L., and Hereld, M. 1990, preprint.